Journal of Materials Chemistry A

Accepted Manuscript

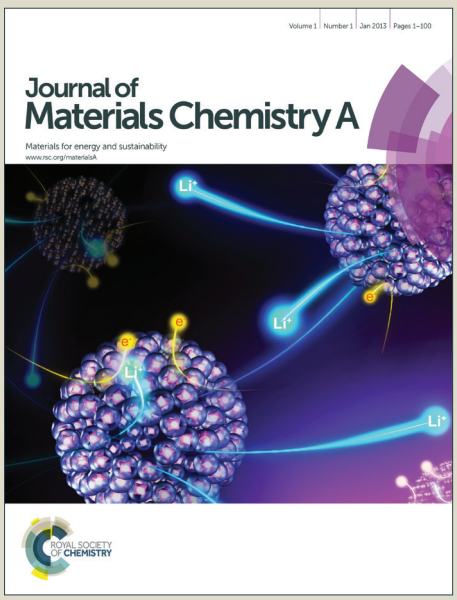

ROYAL SOCIETY OF CHEMISTRY

www.rsc.org/materialsA

Journal Name
Journal of Materials Chemistry A
Dynamic Article Links ►

Cite this: DOI: 10.1039/c0xx00000x

www.rsc.org/xxxxxx

ARTICLE TYPE

Self-seeded growth of nest-like hydrated tungsten trioxide film directly on FTO substrate for highly enhanced electrochromic performance

Haizeng Li,[a] Guoying Shi,[c] Hongzhi Wang,*[a] Qinghong Zhang[b] and Yaogang Li*[b]

Received (in XXX, XXX) Xth XXXXXXXXX 20XX, Accepted Xth XXXXXXXXX 20XX
DOI: 10.1039/b000000x

Self-seeded hydrothermal process could eliminate the grain boundaries existing in the nanocrystalline base layer, speeding up electron transport to the fluorine-doped tin oxide (FTO) glass and promoting electron transfer efficiency. This report highlights the hierarchical nest-like $WO_3 \cdot 0.33H_2O$ film grown directly on bare FTO glass without a seed layer prepared in advance. The film exhibits highly improved electrochromic performances.

Introduction

Electrochromic (EC) materials are capable of reversibly and persistently changing their optical properties under an external voltage, and are considered to be one of the most promising candidates for energy-saving smart (ESS) windows. In recent years, tungsten oxide (WO_3) has attracted immense attention for its distinctive properties, such as water splitting,[1,2] gas sensing,[3,4] photocatalytic degradation[5] and electrochromism.[6] As a traditional EC material, WO_3 exhibits fairly good optical modulation and high cyclic stability. Therefore, a lot of researches have been done to synthesize WO_3 films for electrochromic device.

A great deal of efforts have been taken on preparing high-performance WO_3 films, especially nanoscale porous tungsten oxide films. Traditionally, WO_3 film was fabricated on a transparent conductive substrate to form a working electrode via a number of methods, such as sol–gel reaction method,[7] sputtering[8] and anodic growth method.[9] However, we should recognize that each of these methods mentioned above has one or more characteristic drawbacks, including high-energy consumption, leading to inconvenience of large area fabrication and poor EC stability. The hydrothermal approach is a facile, dominant tool for the synthesis of crystalline oxides, which is promising for the fabrication of WO_3 films because of its advantages, which include control over the size, low reaction temperatures and cost-effectiveness. [10-12]

In recent years, research on two dimensional (2D) nanosheets has intensified significantly after the discovery of graphene.[13-18] 2D materials are considered one of the most promising electrode materials owing to their lamellar permeable spaces, large surface area, and high electrical conductivity.[19,20] As is well known, electrochromic performance mainly depends on the ionic diffusion in an electrochromic material. Thus, 2D WO_3 (hydrate), with high surface ratio and permeable channels, could significantly enhance EC performance.[21] 2D WO_3 (hydrate) can be obtained by various techniques including high-temperature anodization,[22] as well as by hydrothermal,[23,24] acid etching,[25] laser ablation,[26] and exfoliation.[21,27] Our group has made comprehensive studies about crystal-seed-assisted hydrothermal technique in preparing WO_3 nanoflake films.[28] However, the high reaction temperature and long cycle of crystal-seed-assisted hydrothermal process hinder researches and applications of the hydrothermal technique. Besides, the current crystal-seed-assisted hydrothermal process typically needs a fairly complicated process for preparing the seed layer.[28-30] And the seed layer would highly increase energy consumption not only in preparation, but includes applications of electrode. Moreover, the seed layer with poor qualities could lead a worse WO_3 electrode. Herein, we optimize the typical hydrothermal technique in this paper and prepare a uniform nest-like nanosheets WO_3 (hydrate) film directly on bare fluorine-doped tin oxide (FTO) glass without a seed layer prepared in advance. Compared with the electrode prepared by crystal-seed-assisted hydrothermal technique, the as-prepared electrode could essentially improve the energy efficiency and shows a markedly shortened response time.

Results and discussion

Structure and morphology analysis

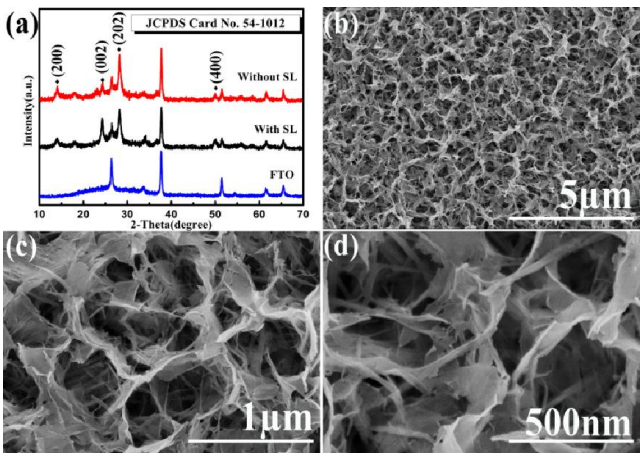

Fig. 1 (a) XRD pattern of as-obtained $WO_3 \cdot 0.33H_2O$ electrode. FE-SEM images of as-obtained $WO_3 \cdot 0.33H_2O$ electrode without SL prepared in advance: (b) low magnification, (c) higher magnification and (d) partial enlarged views.

In a typical procedure, a bare FTO glass and a peroxopolytungstic acid precursor were hydrothermally treated at 120 °C for 2 h. Fig. 1a shows the X-ray powder diffraction (XRD) patterns of the bare FTO glass and the as-obtained films grown with and without a 300 nm-thick WO_3 seed layer deposited on an FTO-coated glass substrate via a typical spin-coating method.[28] The XRD pattern of the FTO glass can be clearly indexed to tin oxide (JCPDS Card No. 70-4176) and the as-obtained films have the same crystalline structure since all diffraction peaks appear at the same position. The Raman spectra indicate that the as-prepared films are WO_3 hydrates (see Fig. S1 in ESI), and all peaks of the hydrothermally grown films can be well indexed to the orthorhombic phase of $WO_3{\cdot}0.33H_2O$ (JCPDS Card No. 54-1012). The sharp peaks indicate the good crystalline quality of the as-fabricated films. However, the relative peak intensity for crystalline plane of (002) of the film grown without SL prepared in advance is different from the one with SL, indicating different preferred growing direction due to the directing effect of SL. The orthorhombic $WO_3{\cdot}0.33H_2O$ contains two types of corner-sharing WO_6 octahedron. One type is constructed by a central tungsten atom that is surrounded by six oxygen atoms, while in the second type, two of the oxygen atoms are replaced by a shorter terminal W=O bond and a longer W–$(OH)_2$ bond, respectively.[31] The relatively weaker interaction between adjacent layers may restrict the stacking to prevent the bulk formation.[23] Finally, the 2D $WO_3{\cdot}0.33H_2O$ nanosheets are formed.

The morphologies of as-obtained electrode without SL prepared in advance are shown in Fig. 1(b,c,d), which exhibit a large area and uniform hierarchical nanostructured thin film composed of nest-like nanosheets and nanoribbons. As shown in Fig. 1(d), the nanonests are formed of 2D nanonests and nanoribbons, which is different from the hydrothermally grown films with SL (see Fig. S2 in ESI). The nanoribbons could highly increase the specific surface area and lead a beneficial effect on the kinetics of lithium insertion into tungsten oxide. The lateral size of the 3D nanonests is larger than 500 nm (Fig. 1(c)), so that the contact area between the film and electrolyte can be largely increased. These hierarchical 2D nanosheets and nanoribbons with high surface ratio and permeable channels could maximize the utilization ratio of $WO_3{\cdot}0.33H_2O$ and reduce diffusion paths of the ions significantly, ions in the electrolyte can diffuse more easily and efficiently. Therefore, the as-obtained electrode could markedly shorten the response time of the electrochromic device (ECD), which is a crucial parameter for practical devices.

Proposed formation mechanism

To further understand the growth mechanism of the as-obtained $WO_3{\cdot}0.33H_2O$ electrode, we examined the crosssectional views of the electrode prepared without SL. From the crosssectional views of the film, it is found that the nanoribbon bundles grow vertically on the substrate at the bottom of the film (Fig. 2(a,b,c)), and the microstructures of nanoribbons are changed into 2D nanosheets at the top of the film. So, based on the above analyses, we provide a possible growth mechanism for the formation of the $WO_3{\cdot}0.33H_2O$ film prepared without SL. The formation mechanism of the as-obtained SL free $WO_3{\cdot}0.33H_2O$ is thought to be a multistep growth process. It follows a self-seed – nanoribbon bundles – nanonests growth mechanism, which is illustrated in Fig. 2(d). Firstly, H_2WO_4 was dissolved via the addition of H_2O_2 to form peroxopolytungstic acid (PTA).[29] Then, $WO_3{\cdot}0.33H_2O$ crystal nuclei was obtained when the reaction temperature exceeded the decomposition temperature of PTA.[23,32] Meanwhile, ethylene glycol (EG) adsorbed on the $WO_3{\cdot}0.33H_2O$ crystal nuclei via hydrogen bonds or physical adsorption,[33] and EG acted as a bridge between the FTO glass and $WO_3{\cdot}0.33H_2O$ crystal nuclei. As a consequence, a self-seeded seed dots layer (SDL) was formed on the surface of FTO glass. Subsequently, the nanoribbons were preferred orientation grown on the self-seeded SDL from the precursor and finally gathered together over time. The third stage was the formation of the nest-like nanosheets, the structures were built from nanoribbon bundles as the second order structure in a self-assembled manner. So, we define this facile hydrothermal technique as a novel self-seeded hydrothermal technique based on the analyses mentioned above.

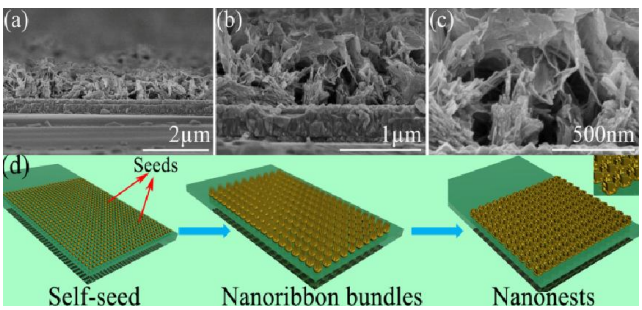

Fig. 2 Crosssectional views of $WO_3{\cdot}0.33H_2O$ electrode prepared without SL: (a) Low magnification, (b) higher magnification and (c) partial enlarged view. (d) A schematic illustration of the formation process for the as-obtained $WO_3{\cdot}0.33H_2O$ electrode prepared without SL.

The components of the solvent also play an important role in growing the various morphologies of the $WO_3{\cdot}0.33H_2O$ films. To further understand the effect on $WO_3{\cdot}0.33H_2O$ morphologies with different solvent components of the self-seeded growth technique, we examined the morphologies of self-seeded grown tungsten oxide film with less amount of ethylene glycol (Fig. 3). The FE-SEM images of $WO_3{\cdot}0.33H_2O$ nanoribbon films shown in Fig. 3 are self-seeded grown using an H_2WO_4 (0.1 M, 10.5 mL) solution, with HCl (3 M, 3.5 mL) and de-ionized water (14 mL) added to ethylene glycol (28 mL). Thus, It can be concluded from the comparative experiments that the nanoribbons of self-seeded grown tungsten oxide film will transform into nest-like nanosheets as the amount of ethylene glycol in the mixed solvent increased.

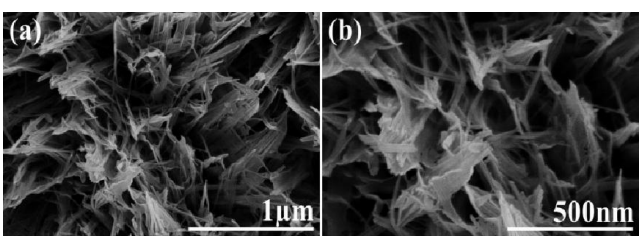

Fig. 3 FE-SEM images of self-seeded grown $WO_3{\cdot}0.33H_2O$ electrode with less amount of ethylene glycol: (a) Low magnification, (b) higher magnification.

Electrochromic and electrochemical properties

Besides the simpleness and convenience exhibited in the facile self-seeded hydrothermal technique, the as-obtained electrode

also exhibits reasonably good electrochromic performance. The EC phenomena of the self-seeded grown electrode were measured at room temperature using the CHI-760D electrochemical workstation via a three-electrode configuration in 1 M lithium perchlorate ($LiClO_4$) – propylene carbonate (PC) electrolyte solution, employing the as-obtained electrode as working electrode and a Pt wire (0.5 mm diameter) as the counter electrode, together with an Ag/AgCl (3 M KCl) reference electrode. The UV-vis transmittance spectra and EC phenomena are shown in Fig. 4. The photographs shown in Fig. 4(b) reveal that the logo placed below the film can be seen clearly, indicating that the film is transparent enough. It can be seen that the color deepened with the voltage changed from − 0.5 V to − 1.0 V. The UV-vis transmittance spectra of the self-seeded grown film in the colored and bleached states were measured at − 0.5 V, − 1.0 V and + 1.0 V, respectively, for 60 s (Fig. 4(a)). The transmittance of the self-seeded grown film at 632.8 nm is measured to be ~ 68% when bleached. Besides the high transmittance of the bleached state, the self-seeded grown film has a fairly high modulation range when colored at a very low voltage. The modulation ranges of the self-seeded grown film at 632.8 nm after applying voltages of − 0.5 and − 1.0 V are calculated to be 40.8 and 57.6 %, respectively. The modulation range calculated at − 0.5 V of the self-seeded grown film is 27 % higher than that of the crystal-seed-assisted film (see Fig. S3 in ESI) and approximately equal to the result in previous report when colored at − 2 V for 60 s.[28]

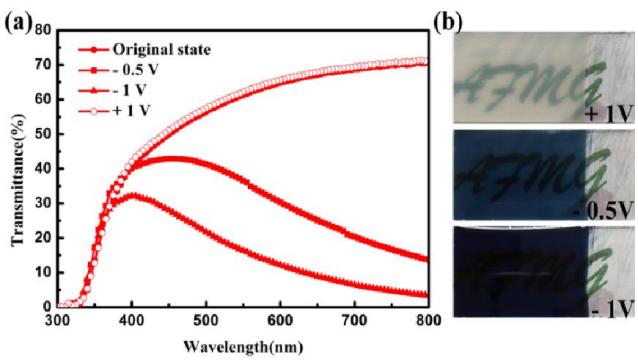

Fig. 4 (a) UV-vis transmittance spectra of the self-seeded grown $WO_3 \cdot 0.33H_2O$ film measured at −0.5 V, −1.0 V and +1.0 V, respectively. (b) Digital photographs of the self-seeded grown $WO_3 \cdot 0.33H_2O$ film.

To investigate the cause of the fairly good EC phenomenon, cyclic voltammetry curves were recorded for the self-seeded grown electrode and crystal-seed-assisted grown electrode at room temperature via the above three-electrode configuration; these are shown in Fig. 5(a). It can be seen that the anodic peak of self-seeded grown film is 53 % higher than that of the crystal-seed-assisted grown film, and the cathodic peak has raised by 44 percent. This good electrochemical performance can be attributed to the novel SL free self-seeded hydrothermal process, which can eliminate the grain boundaries existing in the nanocrystalline base layer, speeding up electron transport to the conductive substrate and promoting electron transfer efficiency.[34] The schematic illustration of the electron transport process is shown in Fig. 5(b). Besides, 2D structures of the electrode make ions in the electrolyte can diffuse more easily and efficiently, so that there will be more Li^+ ions insert into the $WO_3 \cdot 0.33H_2O$ film at a low voltage.

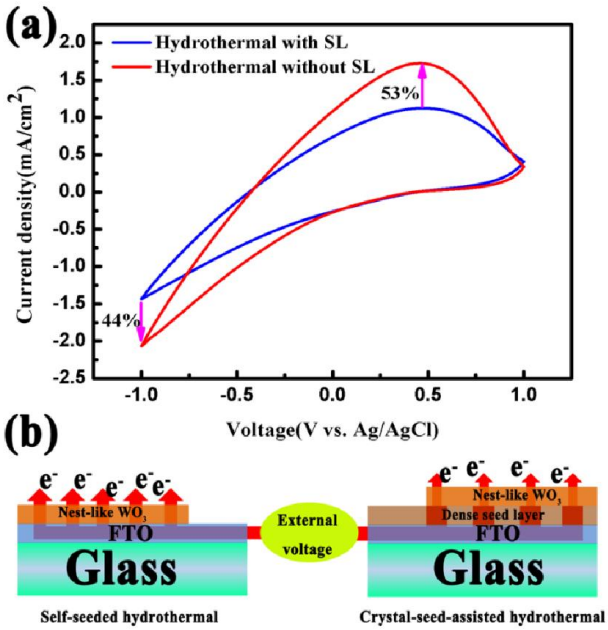

Fig. 5 (a) Cyclic voltammetry curves of the self-seeded grown $WO_3 \cdot 0.33H_2O$ film and crystal-seed-assisted $WO_3 \cdot 0.33H_2O$ film, measured in 1.0 M lithium perchlorate-PC solution between −1.0 and 1.0 V at a sweep rate of 100 mV/s. (b) Schematic illustration of electron transport process.

The switching time characteristics of the self-seeded grown $WO_3 \cdot 0.33H_2O$ film are shown in Fig. 6(a). The coloration and bleaching times are defined as the time required for 90 % change in the entire transmittance modulation. The coloration time t_c and bleaching time t_b are found to be 26 s and 5.5 s respectively, which are faster than those previous reports.[32,35] Compared with the crystal-seed-assisted grown film, the coloration time of the self-seeded grown film is shrunk by 28 % (see Fig. S4(a) in ESI). The fast switching speed of the self-seeded grown film is the result of the hierarchical 2D structures and grain boundary elimination of the nanocrystalline base layer, which make it easier for the Li^+ ion intercalation processe to complete.

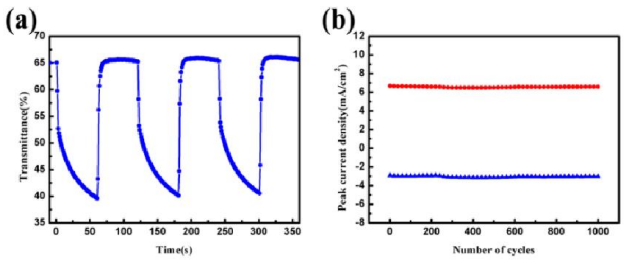

Fig. 6 (a) Switching time characteristics between the colored and bleached states for self-seeded grown $WO_3 \cdot 0.33H_2O$ film measured at 632.8 nm, ± 3.0 V bias.. (b) Peak current evolution of self-seeded grown $WO_3 \cdot 0.33H_2O$ film during the step chronoamperometric cycles.

Electrochemical stability is another essential parameter for EC materials. The electrochemical stability of the self-seeded grown film was characterized by chronoamperometry using square potentials (between −1.0 and 1.0 V). The peak current density of each cycle is recorded in Fig. 6(b). Compared with the crystal-seed-assisted grown film, the self-seeded grown film has no

significant difference in cycle stability, indicating that hydrothermal without SL prepared in advance do no harm to the electrochemical stability of $WO_3 \cdot 0.33H_2O$ electrodes (see Fig. S4(b) in ESI).

Coloration efficiency (CE), which is defined as the change in optical density (ΔOD) per unit of charge (ΔQ) intercalated into the EC layers, is a crucial characteristic parameter for comparing the EC performance of the materials.[36] The CE of self-seeded grown electrode is calculated to be 126.34 cm^2C^{-1} (see Fig. S5 in ESI), which is higher than that of the crystal-seed-assisted grown film and some earlier reports.[12,29] The high coloration efficiency of the as-synthesized $WO_3 \cdot 0.33H_2O$ film is mainly correlated with its 2D nanosheets structure and nest-like morphology. Besides, the novel SL free self-seeded hydrothermal process can also improve the CE of the electrode for the improved electron transfer efficiency.

Conclusions

In summary, nest-like $WO_3 \cdot 0.33H_2O$ films are assembled directly on a FTO glass substrate via a novel and facile self-seeded hydrothermal method. Compared with the crystal-seed-assisted grown film, the self-seeded film shows significantly improved EC performance caused by its unique self-seeded hydrothermal technique, which can eliminate the grain boundaries existing in the nanocrystalline base layer, speeding up electron transport to the FTO glass and promoting electron transfer efficiency. Besides, hierarchical nanoribbons were appeared under this self-seeded hydrothermal process, which provide larger active surface area and therefore led to the self-seeded films with improved electrochromic performance. Moreover, 2D structures can also significantly enhance EC performance. Such $WO_3 \cdot 0.33H_2O$ films with improved EC behaviors, which could essentially improve energy efficiency, possess promising implications for potential applications in energy-saving smart windows and displays.

Experimental Section

Preparation of Precursor and Hydrothermal Treatment

All solvents and chemicals were of analytical grade and were used without further purification. The self-seeded growth of nest-like $WO_3 \cdot 0.33H_2O$ film was synthesized on a FTO glass using a hydrothermal technique. The precursor solution for hydrothermal use was prepared by dissolving H_2WO_4 (5 g) in 30 wt% H_2O_2 (60 mL), while heating at 95 °C with stirring. The resulting clear solution was diluted using de-ionized water to 200 mL, giving a concentration of 0.1 M. The nest-like films were grown using an H_2WO_4 (0.1 M, 10.5 mL) solution, with HCl (3 M, 3.5 mL) and de-ionized water (10.5 mL) added to ethylene glycol (31.5 mL). The mixture was transferred into a 70 mL Teflon-lined stainless-steel autoclave, holding a vertically oriented FTO glass; the autoclave was then sealed and maintained at 120 °C for 2 h. We have chosen the temperature of 120 °C for the hydrothermal reaction because it is low but higher than the normal boiling point of the 60 % (by volume) ethylene glycol solution (~ 110°C, see Fig. S6 in ESI), ensuring enhanced dilution capability through intensified molecular motion.[37] The FTO glass was finally rinsed with absolute alcohol and de-ionized water, and dried in atmosphere. For comparison, a WO_3 film was prepared on a seed layer coated FTO glass via the same hydrothermal process (crystal-seed-assisted hydrothermal method).

Preparation of seed layer

Preparation of seed solution

The seed solution was made by adding a 3 M HCl solution to a 0.2 M $Na_2WO_4 \cdot 2H_2O$ aqueous solution until no more precipitate was formed. Afterwards, cold water was used to wash the precipitate with centrifugation of 8000 rpm for 10 min again and again. Finally, the washed precipitate was dissolved with 30 wt% H_2O_2 drop by drop.

Preparation of seed layer

The seed layer coated FTO glass was prepared via a spin-coating method, as described in our previous work.[28,29] WO_3 seed layer was deposited on an FTO coated glass substrate (cleaned using acetone, ethanol, and deionized water, sequentially) by spin-coating a seed solution, followed by annealing at 400 °C for 1 h.

Characterization

The morphology of the electrode was observed via a S-4800 field-emission scanning electron microscope (Hitachi, Tokyo, Japan) operated at 5 kV. Electrodes were investigated using an powder X-ray diffraction technique (XRD, D/max 2550 V, Rigaku, Tokyo,Japan) with Cu Ka(λ= 1.5406A°) radiation at 40 kV and 300 mA. Raman spectra were recorded on a Renishaw in plus laser Raman spectrometer with λexc=432 nm. The transmittance spectra and the coloration/bleaching time of the electrodes were measured by Lambda 950 (Perkin Elmer, Waltham, MA, USA). Electrochemical measurements were carried out on the CHI760D (Shanghai Chenhua Instruments, China) electrochemical workstation.

Acknowledgements

We gratefully acknowledge the financial support by Natural Science Foundation of China (No. 51172042), Specialized Research Fund for the Doctoral Program of Higher Education（20110075130001），Science and Technology Commission of Shanghai Municipality (12nm0503900,13JC1400200), the Program for Professor of Special Appointment (Eastern Scholar) at Shanghai Institutions of Higher Learning, Innovative Research Team in University（IRT1221）and the Program of Introducing Talents of Discipline to Universities (No.111-2-04).

Notes and references

[a] *State Key Laboratory for Modification of Chemical Fibers and Polymer Materials, College of Materials Science and Engineering, Donghua University, Shanghai 201620, P. R. China. E-mail: wanghz@dhu.edu.cn; Fax: +86-021-67792855; Tel: +86-021-67792881*

[b] *Engineering Research Center of Advanced Glasses Manufacturing Technology, Ministry of Education, College of Materials Science and Engineering, Donghua University, Shanghai 201620, P. R. China. E-mail: yaogang_li@dhu.edu.cn; Fax: +86-021-67792855; Tel: +86-021-67792526*

[c] *College of Chemistry, Chemical Engineering and Biotechnology, Donghua University, Shanghai 201620, China*

† Electronic Supplementary Information (ESI) available: [details of any supplementary information available should be included here]. See DOI: 10.1039/b000000x/

‡ Footnotes should appear here. These might include comments relevant to but not central to the matter under discussion, limited experimental and spectral data, and crystallographic data.

1 D. Chandra, K. Saito, T. Yui and M. Yagi, *Angew. Chem. Int. Ed.*, 2013, **52**, 12606.
2 R. Abe, K. Shinmei, N. Koumura, K. Hara and B. Ohtani, *J. Am. Chem. Soc.*, 2013, **135**, 16872.
3 H. G. Moon, Y. S. Shim, D. H. Kim, H. Y. Jeong, M. Jeong, J. Y. Jung, S. M. Han, J. K. Kim, J. S. Kim, H. H. Park, J. H. Lee, H. L. Tuller, S. J. Yoon and H. W. Jang, *Sci. Rep.*, 2012, **2**, 588.
4 S. Vallejos, P. Umek, T. Stoycheva, F. Annanouch, E. Llobet, X. Correig, P. D. Marco, C. Bittencourt and C. Blackman, *Adv. Funct. Mater.*, 2013, **23**, 1313.
5 D. Vernardou, H. Drosos, E. Spanakis, E. Koudoumas, C. Savvakis and N. Katsarakis, *J. Mater. Chem.*, 2011, **21**, 513.
6 C. G. Granqvist, *Sol. Energy Mater. Sol. Cells*, 2000, **60**, 201.
7 L. Yang, D. Ge, J. Zhao, Y. Ding, X. Kong and Y. Li, *Sol. Energy Mater. Sol. Cells*, 2012, **100**, 251.
8 X. Yang, G. Zhu, S. Wang, R. Zhang, L. Lin, W. Wu and Z. L. Wang, *Energy Environ. Sci.*, 2012, **5**, 9462.
9 J. Z. Ou, S. Balendhran, M. R. Field, D. G. McCulloch, A. S. Zoolfakar, R. A. Rani, S. Zhuiykov, A. P. O'Mullane and K. Kalantar-zadeh, *Nanoscale*, 2012, **4**, 5980.
10 J. Zhang, J. P. Tu, X. H. Xia, X. L. Wang and C. D. Gu, *J. Mater. Chem.*, 2011, **21**, 5492.
11 W. Xiao, W. Liu, X. Mao, H. Zhu and D. Wang, *J. Mater. Chem. A*, 2013, **1**, 1261.
12 J. Wang, E. Khoo, P. S. Lee and J. Ma, *J. Phys. Chem. C*, 2009, **113**, 9655.
13 Q. H. Wang, K. Kalantar-zadeh, A. Kis, J. N. Coleman and M. S. Strano, *Nat. Nanotechnol*, 2012, **7**, 699.
14 S. Balendhran, J. Z. Ou, M. Bhaskaran, S. Sriram, S. Ippolito, Z. Vasic, E. Kats, S. Bhargava, S. Zhuiykov and K. Kalantar-zadeh, *Nanoscale*, 2012, **4**, 461.
15 S. Balendhran, J. Deng, J. Z. Ou, S. Walia, J. Scott, J. Tang, K. L. Wang, M. R. Field, S. Russo, S. Zhuiykov, M. S. Strano, N. Medhekar, S. Sriram, M. Bhaskaran and K. Kalantar-zadeh, *Adv. Mater.*, 2013, **25**, 109.
16 K. Kalantar-zadeh, J. Tang, M. Wang, K. L. Wang, A. Shailos, K. Galatsis, R. Kojima, V. Strong, A. Lech, W. Wlodarski and R. B. Kaner, *Nanoscale*, 2010, **2**, 429.
17 S. Balendhran, S. Walia, H. Nili, J. Z. Ou, S. Zhuiykov, R. B. Kaner, S. Sriram, M. Bhaskaran and K. Kalantar-zadeh, *Adv. Funct. Mater.*, 2013, **23**, 3952.
18 S. Balendhran, S. Walia, M. Alsaif, E. P. Nguyen, J. Z. Ou, S. Zhuiykov, S. Sriram, M. Bhaskaran and K. Kalantar-zadeh, *ACS nano*, 2013, **7**, 9753.
19 J. Feng, X. Sun, C. Wu, L. Peng, C. Lin, S. Hu, J. Yang and Y. Xie, *J. Am. Chem. Soc.*, 2011, **133**, 17832.
20 J. Xie, X. Sun, N. Zhang, K. Xu, M. Zhou and Y. Xie, *Nano Energy*, 2013, **2**, 65.
21 L. Liang, J. Zhang, Y. Zhou, J. Xie, X. Zhang, M. Guan, B. Pan and Y. Xie, *Sci. Rep.*, 2013, **3**, 1936.
22 A. Z. Sadek, H. Zheng, M. Breedon, V. Bansal, S. K. Bhargava, K. Latham, J. Zhu, L. Yu, Z. Hu, P. G. Spizzirri, W. Wlodarski and K. Kalantar-zadeh, *Langmuir*, 2009, **25**, 9545.
23 Z. Jiao, X. Wang, J. Wang, L. Ke, H. V. Demir, T. W. Koh and X. W. Sun, *Chem. Commun.*, 2012, **48**, 365.
24 F. Amano, M. Tian, G. Wu, B. Ohtani and A. Chen, *ACS Appl. Mater. Interfaces*, 2011, **3**, 4047.
25 E. Widenkvist, R. A. Quinlan, B. C. Holloway, H. Grennberg and U. Jansson, *Cryst. Growth Des.*, 2008, **8**, 3750.
26 H. Zhang, G. Duan, Y. Li, X. Xu, Z. Dai and W. Cai, *Cryst. Growth Des.*, 2012, **12**, 2646.
27 K. Kalantar-zadeh, A. Vijayaraghavan, M. H. Ham, H. Zheng, M. Breedon and M. S. Strano, *Chem. Mater.*, 2010, **22**, 5560.
28 D. Ma, H. Wang, Q. Zhang and Y. Li, *J. Mater. Chem.*, 2012, **22**, 16633.
29 D. Ma, G. Shi, H. Wang, Q. Zhang and Y. Li, *J. Mater Chem. A*, 2013, **1**, 684.
30 G. Wang, Y. Ling, H. Wang, X. Yang, C. Wang, J. Z. Zhang and Y. Li, *Energy Environ. Sci.*, 2012, **5**, 6180.
31 H. Zheng, J. Z. Ou, M. S. Strano, R. B. Kaner, A. Mitchell and K. Kalantar-zadeh, *Adv. Funct. Mater.*, 2011, **21**, 2175.
32 Z. Jiao, X. W. Sun, J. Wang, L. Ke and H. V. Demir, *J. Phys. D: Appl. Phys.*, 2010, **43**, 285501.
33 J. Li, L. Zhu and X. Liu, *New J. Chem.*, 2013, **37**, 4241.
34 J. Yang, W. Li, J. Li, D. Sun and Q. Chen, *J. Mater. Chem.*, 2012, **22**, 17744.
35 J. M. Wang, E. Khoo, P. S. Lee and J. Ma, *J. Phys. Chem. C*, 2008, **112**, 14306.
36 D. D. Yao, R. A. Rani, A. P. O'Mullane, K. Kalantar-zadeh and J. Z. Ou, *J. Phys. Chem. C*, 2014, **118**, 476.
37 M. Trapatseli, D. Vernardou, P. Tzanetakis and E. Spanakis, *ACS Appl. Mater. Interfaces*, 2011, **3**, 2726.